



Marian Klasztorny^{1*}, Daniel Nycz², Marek Cedrowski³

¹ Military University of Technology, Faculty of Mechanical Engineering, Department of Mechanics & Applied Computer Science, ul. Kaliskiego 2, 00-908 Warsaw, Poland

² DES ART Co. Ltd., Headquarters - Gdynia, Branch Office - Sanok, ul. Lipińskiego 113, 38-500 Sanok, Poland

³ B.Sc. student, Military University of Technology, Faculty of Mechanical Engineering, ul. Kaliskiego 2, 00-908 Warsaw, Poland

*Corresponding author. E-mail: m.klasztorny@gmail.com

Received (Otrzymano) 17.02.2015

MODELLING, SIMULATION AND VALIDATION OF BENDING TEST OF BOX SEGMENT FORMED AS TWO COMPOSITE SHELLS GLUED TOGETHER

The present experimental and numerical research is focused on a box composite beam, so-called a validation segment, consisting of two vinylester/glass shells glued together. The top shell has a hat cross-section, whereas the bottom one is flat. The shells are glued together at two horizontal contact strips. The validation segment reflects the central part of the cross- and longitudinal-section of a box composite superstructure of a footbridge designed by the authors. The dimensions of the cross-section and the number of fabric layers in the validation segment are decreased twice in comparison with the footbridge superstructure. Moreover, the composite beam was rotated by 180° in relation to the footbridge. The validation segment is 2.35 m long, and the cross-section overall dimensions are 0.60 m × 0.26 m (width×height). The laminate components, glue and manufacturing technology of the validation segment are the same as for the composite footbridge. The study develops a methodology for numerical modelling and simulation by the Finite Element Method of box composite girders formed as two composite shells glued together. The methodology is developed in reference to the validation segment which is subjected to the 3-point bending test with shear. Experimental validation of the modelling and simulation was carried out for the basic case of new laminates at 20°C. FE computer code MSC.Marc 2010 was used for the numerical modelling and simulation.

Keywords: thin-walled box beam, GFRP laminate, glue layer, three-point bending test, modelling and simulation, experimental validation

MODELOWANIE, SYMULACJA I WALIDACJA PRÓBY ZGINANIA SEGMENTU SKRZYNKOWEGO W FORMIE DWÓCH POWŁOK KOMPOZYTOWYCH SKLEJONYCH ZE SOBĄ

Przedmiotem badań eksperymentalnych i numerycznych jest belka kompozytowa o przekroju skrzynkowym, zwana segmentem walidacyjnym, składająca się z dwóch sklejoných ze sobą powłok kompozytowych winyloestrowo-szkłanych. Powłoka górna ma przekrój kapeluszowy, a powłoka dolna jest płaska. Powłoki są sklezione ze sobą na dwóch poziomych pasach kontaktu. Segment walidacyjny odwzorowuje środkową część przekroju poprzecznego i podłużnego konstrukcji nośnej kompozytowej skrzynkowej kładki dla pieszych zaprojektowanej przez autorów. Wymiary przekroju poprzecznego oraz liczba warstw tkanin w laminatach segmentu walidacyjnego są dwukrotnie mniejsze w porównaniu z konstrukcją nośną kładki. Ponadto, segment belkowy obrócono o 180° w porównaniu z kładką. Długość segmentu wynosi 2,35 m, a wymiary gabarytowe przekroju poprzecznego są równe 0,60 m × 0,26 m (szerokość × wysokość). Komponenty laminatów, klej oraz technologia wytwarzania segmentu walidacyjnego są takie same jak w przypadku kładki kompozytowej. Opracowano metodykę modelowania numerycznego i symulacji z wykorzystaniem metody elementów skończonych belek kompozytowych w formie dwóch sklejoných ze sobą powłok kompozytowych. Metodyka została opracowana w odniesieniu do segmentu walidacyjnego poddanego trójpunktowemu zginaniu ze ścinaniem. Walidację eksperymentalną modelowania i symulacji przeprowadzono w podstawowym przypadku laminatów nowych w temperaturze 20°C. Do numerycznego modelowania i symulacji zastosowano kod elementów skończonych MSC.Marc 2010.

Słowa kluczowe: cienkościenna belka skrzynkowa, laminat GFRP, warstwa kleju, próba trójpunktowego zginania, modelowanie i symulacja, walidacja eksperymentalna

INTRODUCTION

A new structural design of a composite foot-cycling bridge was proposed in [1]. The bridge span is simply supported, with a theoretical span of 12.00 m and a usable width of 2.50 m. The cross-section of the footbridge is a 5-box open-closed girder, formed by two vinylester/glass shells. The components of the GFRP

laminates are as follows: Firestop BÜFA-S440 flame retardant vinylester resin (producer: BÜFA Gelcoat Plus, Germany); BAT800 [0/90], GBX800 [45/–45] quasi-balanced stitched E-glass fabrics (producer: DIPEX, Slovakia). The laminates are manufactured using infusion technology. Glue joints between the top

and the bottom shells as well as between the cross members and the shells are made using high-strength and vibration-resistant NORPOL FI-184 glue (producer: Reichhold, Norway). The thickness of the adhesive layer is 2 mm. A geometrical model of the considered footbridge in the top isometric view is depicted in Figure 1 (support zone zoomed).

Composite footbridges are constantly being researched and developed in terms of forming, numerical modelling, simulation and design. The Eurocodes for standard footbridges do not include this type of structural materials. Adequate numerical modelling and simulation of static processes play an essential role in the design of footbridges.

The study develops a methodology for numerical modelling and simulation by the Finite Element Method of box composite girders formed as two composite shells glued together. The methodology is developed in reference to the central 1-box segment extracted from the whole footbridge superstructure presented in Figure 1. The test segment has the overall dimensions and number of layers decreased twice compared to the original segment (half scale model). The test segment is subjected to a 3-point bending test with shear. Experimental validation of the modelling and simulation is conducted for the basic case of new laminates at the temperature of 20°C.

The basic approach to modelling polymer-matrix laminates involves homogenization of the layers, i.e. the replacement of heterogeneous material at the micro level (two-component material) with homogeneous material at the macro level. The laminas are modelled approximately as linear orthotropic elastic-brittle materials [2]. The considered laminas are each reinforced with an E-glass balanced stitched fabric. The equivalent homogeneous orthotropic material has orthotropy directions 1, 2, 3 coinciding to the warp, weft and thickness directions, respectively. Each lamina is described by 9 effective elasticity constants:

E_i - Young's modulus in i - direction,

ν_{ij} - Poisson's ratio in ij - plane, $ij = 12, 23, 31$

G_{ij} - shear modulus in ij - plane, $ij = 12, 23, 31$

and 9 effective strength constants:

R_{it}, R_{ic} - tensile and compressive strengths in i - direction, $i = 1, 2, 3$

S_{ij} - shear strength in ij - plane, $ij = 12, 23, 31$

The simplest and a very accurate method constitutes experimental identification of the elastic-strength properties of a respective uniform laminate reflecting laminas.

To assess the strength of the laminate layer in a complex stress state, various strength theories are applied, including: the maximum stresses (Max Stress), maximum strains, Tsai-Wu, Hashin, Hashin Fabric, Hill-Tsai, Hoffman, Chang-Chang, Hill, Malmeister

and others [2-4]. Based on the identification and validation numerical and experimental studies [5] and on the MSC.Marc system recommendations [4], the following hypotheses in the MSC.Marc system have been selected: the Hashin Fabric hypothesis for layers reinforced with balanced stitched fabrics and the Max Stress hypothesis for a glue layer.

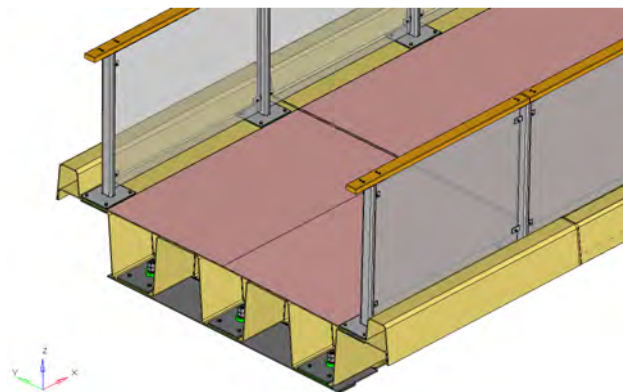


Fig. 1. Composite foot-bicycle bridge - top isometric view [1]

Rys. 1. Kompozytowa kładka pieszo-rowerowa - widok izometryczny z góry [1]

In the case of the Hashin Fabric hypothesis, the following failure indices in each integration point are calculated [4]:

- fibre tension in direction 1, $\sigma_1 > 0$:

$$F_1 = \left[\left(\frac{\sigma_1}{R_{1t}} \right)^2 + \left(\frac{\sigma_{12}}{S_{12}} \right)^2 + \left(\frac{\sigma_{13}}{S_{13}} \right)^2 \right] \quad (1)$$

- fibre compression in direction 1, $\sigma_1 < 0$:

$$F_2 = \left[\left(\frac{\sigma_1}{R_{1c}} \right)^2 + \left(\frac{\sigma_{12}}{S_{12}} \right)^2 + \left(\frac{\sigma_{13}}{S_{13}} \right)^2 \right] \quad (2)$$

- fibre tension in direction 2, $\sigma_2 > 0$:

$$F_3 = \left[\left(\frac{\sigma_2}{R_{2t}} \right)^2 + \left(\frac{\sigma_{12}}{S_{12}} \right)^2 + \left(\frac{\sigma_{23}}{S_{23}} \right)^2 \right] \quad (3)$$

- fibre compression in direction 2, $\sigma_2 < 0$:

$$F_4 = \left[\left(\frac{\sigma_2}{R_{2c}} \right)^2 + \left(\frac{\sigma_{12}}{S_{12}} \right)^2 + \left(\frac{\sigma_{23}}{S_{23}} \right)^2 \right] \quad (4)$$

- matrix tension, $\sigma_3 > 0$:

$$F_5 = \left[\left(\frac{\sigma_3}{R_{3t}} \right)^2 + \left(\frac{\sigma_{12}}{S_{12}} \right)^2 + \left(\frac{\sigma_{13}}{S_{13}} \right)^2 + \left(\frac{\sigma_{23}}{S_{23}} \right)^2 \right] \quad (5)$$

- matrix compression, $\sigma_3 < 0$:

$$F_6 = \left[\left(\frac{\sigma_3}{R_{3c}} \right)^2 + \left(\frac{\sigma_{12}}{S_{12}} \right)^2 + \left(\frac{\sigma_{13}}{S_{13}} \right)^2 + \left(\frac{\sigma_{23}}{S_{23}} \right)^2 \right] \quad (6)$$

where $\sigma_i, \sigma_{ij}, i, j = 1, 2, 3$ - stress tensor components. Each failure index yields a respective effort index calculated according to the following formula

$$R_i = \sqrt{F_i}, \quad i = 1, 2, \dots, 6 \quad (7)$$

The effort indices are the true measure of material effort - they are a measure of distance from the yield surface.

In the case of the Max Stress hypothesis, the following failure indices are calculated [10]:

$$F_i = \begin{cases} \frac{\sigma_i}{R_{it}} & \text{dla } \sigma_i > 0 \\ -\frac{\sigma_i}{R_{ic}} & \text{dla } \sigma_i < 0 \end{cases}, \quad i = 1, 2, 3 \quad (8)$$

$$F_{ij} = \frac{|\sigma_{ij}|}{s_{ij}}, \quad ij = 12, 23, 31$$

In this case, the effort indices are equal to the failure indices, i.e. $R_i = F_i$, $R_{ij} = F_{ij}$, $i, j = 1, 2, \dots, 6$. In addition, the following notation is introduced: $R_4 = R_{12}$, $R_5 = R_{23}$, $R_6 = R_{31}$.

The numerical modelling of mixed laminate shells was developed by the authors in [5, 6]. Study [5] considers the numerical modelling and simulation of static processes, including progressive failure, for GFRP (glass fibre reinforced plastic) laminates of a mixed sequence of laminas reinforced with E-glass plain weave fabric and E-glass mat. The examined laminate was manufactured with contact technology using polyester resin as the matrix. The purpose of the research was to determine the options/values, recommended in engineering calculations, of the parameters for numerical modelling and simulation of static processes including failure for beam, plate and shell structures built of composites undertaken, using FE code MSC.Marc [4].

The 3-point bending test was performed in [6] for a single-wave glass-polyester laminate segment. The geometry and ply sequence of the segment are modelled on the selected composite tank cover. The main purpose of the research was to develop numerical modelling and simulation methodology for such a test using FE code MSC.Marc as well as to perform experimental validation. The numerical tests included the application of six selected shell finite elements which accept layered composite materials, available in the MSC.Marc FE library [4]. It was pointed out that Element_75 (Bilinear Thick Shell) gives results closest to reality, both qualitatively and quantitatively. A set of options/values of numerical modelling and simulation parameters determined in [5] is applied in the present study.

EXPERIMENTAL BENDING TEST OF VALIDATION SEGMENT

A beam composite segment of the box cross-section shown in Figure 2 was chosen for examination. The overall dimensions are as follows: 2350×600×258 mm. The segment includes a top composite shell (TS) and bottom composite shell (BS) glued together at the contact surface using a 0.5 mm thick layer. The top shell has a hat cross-section, whereas the bottom one is flat. The components of the top and bottom shell laminates are specified in the Introduction. A single BAT or GBX fabric corresponds to one lamina. The ply sequence for

the TS and BS laminates is $[\text{BAT}/\text{GBX}/\text{BAT}]_2 = [0/45/0]_2$, wherein only the fabric warp orientation is reflected. The following interpretation of angles is assumed:

- 0 - direction parallel to the beam axis (warp direction in BAT800 fabric)
- 90 - direction perpendicular to the beam axis (weft direction in BAT800 fabric)
- 45/-45 - directions at 45° to the beam axis (warp and weft directions in GBX800 fabric).

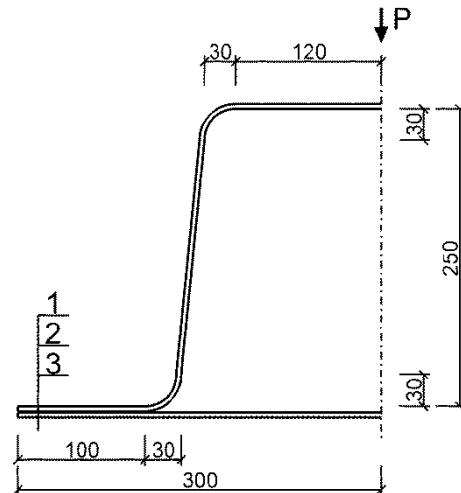


Fig. 2. Cross-section of validation segment: 1 - top shell TS (4 mm), 2 - adhesive layer (0.5 mm), 3 - bottom shell BS (4 mm)

Rys. 2. Przekrój poprzeczny segmentu walidacyjnego: 1 - powłoka górna TS (4 mm), 2 - warstwa kleju (0,5 mm), 3 - powłoka dolna BS (4 mm)

The average thickness of a lamina is 0.663 mm, thus the design thickness of the TS and BS laminate shells is: $6 \times 0.663 \text{ mm} \approx 4.00 \text{ mm}$. The shells were made separately using infusion technology and glued together.

Figure 3 depicts the diagram of the experimental stand for the 3-point bending test of the validation segment. The stand was embedded in a SATEC-1200 universal testing machine. The steel supports were made from an IPE300 I-beam with stiffening ribs arranged transversely to the axis of the segment. A 20 mm thick steel plate was attached to the top flange. The contact edge of the plate was chamfered with a radius of 5 mm. The transverse support I-beams were based on I200 longitudinal steel I-beams located on the rigid bottom table of the machine. The supports have low vertical susceptibility which was controlled by an LK-G157 laser sensor equipped with an LK-GD500 controller.

The 3-point bending test was conducted at kinematic excitation over a vertical distance of 300 mm at a crosshead speed of 1 mm/s. Force (P), crosshead position (s) and vertical displacement of the right support were recorded at a 10 Hz sampling frequency using a Traveler ESAM CF strain gauge bridge. Longitudinal strain gauges EA-16-240LZ-120/E were glued to the bottom surface of the segment at the midspan and at the half-width strips of the adhesive layer.

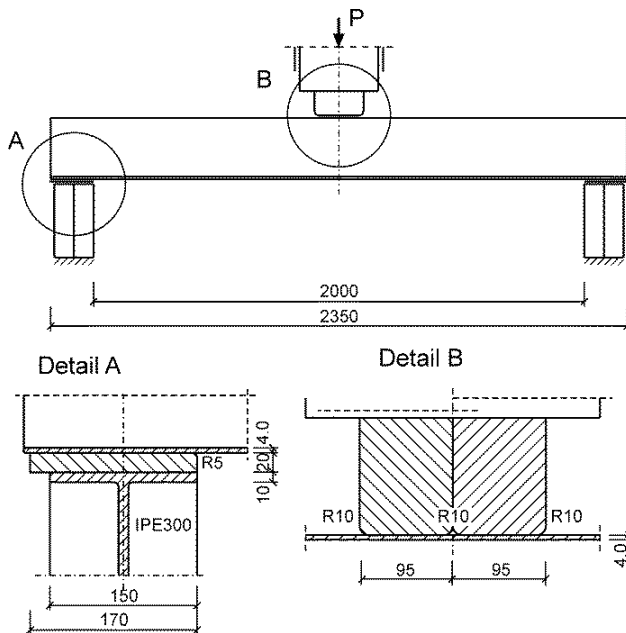


Fig. 3. Diagram of stand for 3-point bending test of validation segment
Rys. 3. Schemat stanowiska do zginania trójpunktowego segmentu walidacyjnego

Figure 4 shows deformation of the segment at a 200 mm vertical displacement of the stamp. Large deformations and damages of the segment appear in the stamp area only. After completion of the loading ($s = 300$ mm), a return to the original geometric shape was observed. It indicates that buckling of the vertical walls occurred in the central zone of the segment during the bending process.

The $P(s)$ plot of the stamp force (P) versus the crosshead displacement (s) is presented in Figure 5. In the range of $0 \div 22$ mm, the response of the girder is quasi-linearly elastic. The load capacity of the segment is $P = 28.8$ kN at the crosshead displacement of 22.0 mm. Afterwards, gradual loss of the load capacity with periodic increases is observed. The response in this range is non-linear with a large number of chart folds corresponding to progressive local destruction of the segment, particularly in the stamp zone.

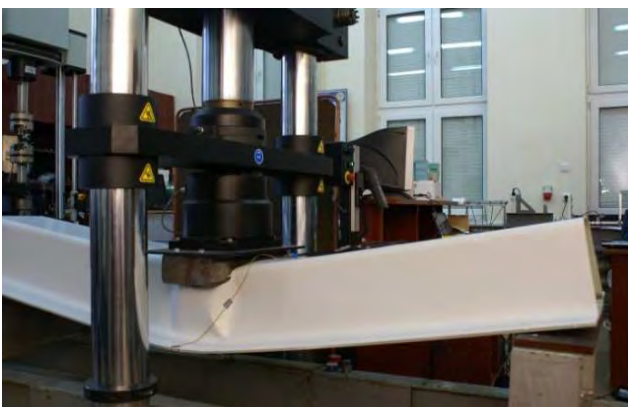


Fig. 4. Deformation of validation segment corresponding to crosshead displacement $s = 200$ mm

Rys. 4. Deformacje segmentu walidacyjnego odpowiadające przemieszczeniu trawersy $s = 200$ mm

Vertical displacement of right support reaches 0.4 mm in the load capacity point. The relative error at this point is $\delta = 0.4/22.02 = 1.8\%$, and it decreases to 0.08% at the end of the test. Therefore, vertical susceptibility of the supports can be omitted in the simulation.

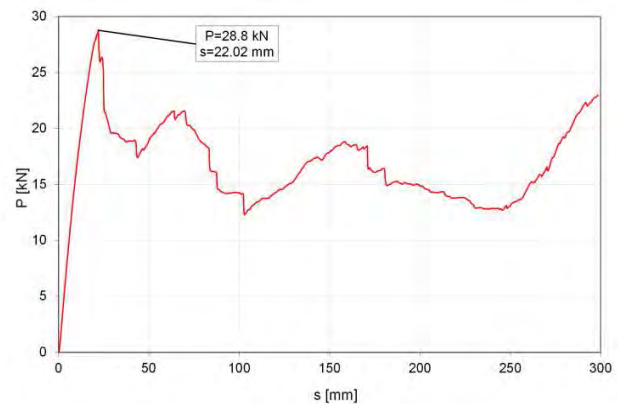


Fig. 5. Stamp force (P) versus crosshead displacement (s)

Rys. 5. Wykres siły nacisku stempla (P) w funkcji przemieszczenia trawersy (s)

NUMERICAL MODELLING AND SIMULATION OF BENDING TEST OF VALIDATION SEGMENT

The FE numerical model of the validation segment was developed in HyperMesh v12.0 software, based on the geometrical model created in the Catia v5r19 system, using the following tools: *Generative Shape Design* (surface modelling), *Part Design* (solid modelling), and *Assembly Design* (assemblies performing). The geometric and material properties, contact, loads and type of analysis were defined in the MSC.Marc 2010 system [4]. In this study, references to the original names of finite elements, parameters and options from the MSC.Marc 2010 system are applied. Selected finite elements, parameters and options are described in a concise manner at the first reference.

The numerical model of the validation segment is shown in Figure 6. QUAD4 shell FEs were used. The basic size of a shell element is 20×20 mm. The element size was reduced to approximately 12×12 mm in the stamp impact zone and chamfered areas. The adhesive layer is one of the layers of the laminates modelled using shell elements. The total number of finite elements and nodes of the segment model is 10836 and 10922, respectively. The supports and movable stamp are modelled as surfaces with perfectly rigid body properties.

Bilinear Thick-Shell Elements (No. 75) are used for composite shell modelling. They are bilinear, 2-dimensional, 4-node shell finite elements having three translational and three rotational degrees of freedom in each node. The transverse shear strains are calculated at the middle of the edges and interpolated to the integration points. The appropriate thickness of the shell and corresponding offsets from the mid-surfaces were defined in the geometrical properties of the FE elements.

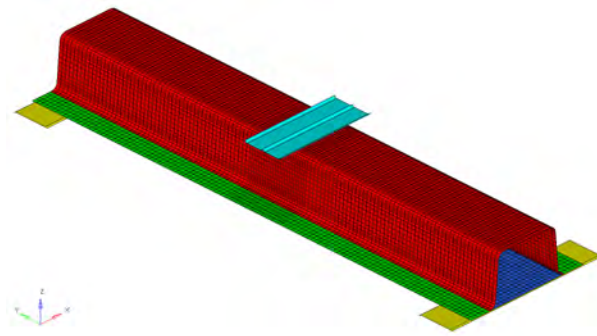


Fig. 6. FE model of validation segment

Rys. 6. Model numeryczny segmentu walidacyjnego

An orthotropic linear elastic-brittle material model was applied for the vinylester/glass lamina (B/F code) whereas an isotropic linear elastic-brittle material model was used with respect to the adhesive layer. The effective material constants of B/F lamina (after homogenization), applied in laminate shells in the [0/90] or [45/-45] configuration, are provided in Table 1, determined from respective experimental tests. The material constants of NORPOL FI-184 glue are provided in Table 2, based on the manufacturer's material card, wherein: E , ν - Young's modulus, Poisson's ratio, R_t - tensile strength, R_c - compressive strength, S - shear strength.

The *Selective Gradual Degradation* model of progressive failure was used with respect to laminate shells. This model decreases the material constants when failure occurs. Within an increment, it attempts to keep the highest failure index less than or equal to 1. Whenever a failure index larger than 1 occurs, the stiffness reduction factor is calculated based upon the value of the failure index.

TABLE 1. Elasticity and strength constants of B/F lamina
TABELA 1. Stałe sprężystości i wytrzymałości laminy B/F

Material constant	Unit	Value
$E_1 = E_2$	[MPa]	23400
ν_{12}	-	0.153
G_{12}	[MPa]	3520
$G_{13} = G_{23}$	[MPa]	2300
$R_{1t} = R_{2t}$	[MPa]	449
$R_{1c} = R_{2c}$	[MPa]	336
S_{12}	[MPa]	45.2
$S_{13} = S_{23}$	[MPa]	27.2

TABLE 2. Material constants for NOPROL FI-184 glue model
TABELA 2. Stałe materiałowe modelu kleju NOPROL FI-184

Material constant	Unit	Value
E	[MPa]	3100
ν	-	0.36
R_t	[MPa]	35.0
R_c	[MPa]	35.0
S	[MPa]	20.3

The contact table was created to define contact. Possible steel - laminate friction pairs were declared in respective subareas of potential contact of the system components. The *Segment-to-Segment* contact model with the *Touching* option, including the Coulomb friction model, was applied. A coefficient of static friction ($\mu = 0.14$) was specified on the basis of the authors' experiments. The *Gravity Load* option was taken into account during the simulation. An acceleration of -9810 mm/s^2 with respect to the vertical axis (Z) of the global coordinate system was declared.

Theoretically, a system for the 3-point bending test of validation segment is perfectly bisymmetric. However, before applying the vertical load, the system is geometrically unstable (horizontal displacements at the supports are possible). Therefore, in order to ensure geometrical stability of the FE model of the validation segment, the translational degrees of freedom in the longitudinal and transverse symmetry planes were fixed. The rotational degrees of freedom were kept since the simulations were carried out with respect to the full numerical model.

The full Newton-Raphson method with the residual convergence criterion (relative tolerance of 0.1) was used to solve the problem. A conventional loading time of 1 s and a constant time step of 0.001 s were applied. Small strains and large rotations were taken into consideration in the calculations. The options/values of the parameters for numerical modelling and simulation of static processes including failure, using the FE code MSC.Marc, assumed in this study, are listed in Table 3.

Figure 7 shows virtual (numerical, simulated) $F(s)$ diagrams against the background of the experimental diagram, corresponding to rare mesh (average size of FE is $20 \times 20 \text{ mm}$) and dense mesh (average size of FE is $10 \times 10 \text{ mm}$). The experimental plot confirms the correctness of the applied material models and values/options of the modelling and simulation parameters listed in Table 3. The experimental and virtual plots are coincident with regard to the initial stiffness. After reaching 18% of the load capacity, the virtual chart exhibits slightly lower stiffness in the range of 18÷36% and above 70% of the load capacity results in a 46% increased displacement of the cross-head at the load capacity point. It results from an undervalued shear modulus, $G_{13} = G_{23}$, which is determined from the approximate 3-point bending test of the short beam.

The differences in virtual plots in the elastic response zone (Fig. 7), corresponding to rare and dense meshes are small whereas the load capacity corresponding to the rare mesh is closer to the experimental values. After reaching the load capacity, progressive destruction begins in the stamp operating zone. The virtual plots are similar to the experimental plot for $s < 250 \text{ mm}$, both qualitatively and quantitatively. Further increasing of the crosshead displacement leads to significant quantitative differences. The reason is the undervalued shear strength, $S_{13} = S_{23}$, determined from the approximate 3-point bending test of the short beam.

It can be assessed that the simulation results corresponding to the rare mesh are validated positively.

TABLE 3. Options/values of parameters for numerical modeling and simulation

TABELA 3. Opcje/wartości parametrów modelowania numerycznego i symulacji

Methodology component	Reference [11]	Presented study
finite element (FE) type	185 (Solid Shell)	75 (Thick Shell)
element size	similar to laminate thickness	20 × 20 mm
failure criteria	Hashin Fabric, Max Stress	Hashin Fabric, Max Stress
failure	progressive	progressive
stiffness degradation method	Gradual Selective	Gradual Selective
residual stiffness factor	0.005	0.1
contact distance tolerance	0.15	automatic
bias factor for distance tolerance	0.95	0.95
friction type	Coulomb bilinear (displacement)	Coulomb bilinear (displacement)
iteration method	Full Newton-Raphson	Full Newton-Raphson
convergence criteria	residual and displacement (0.02)	residual (0.1)
stepping procedure	adaptive	constant (1000 steps)
advanced analysis options	small strain, assumed strain, large rotations	small strain, assumed strain, large rotations

In the virtual plot $P(s)$ in the elastic response zone (Fig. 7), two points (L1, L2) close to the load capacity point (L3) are visible. A slight decrease in force P with an increasing displacement s and re-growth of force P with a further increase in s can be observed in points L1, L2. These points were called the load levels: L1 ($s = 19.5$ mm, $P = 22.6$ kN), L2 ($s = 27.5$ mm, $P = 27.5$ kN), L3 ($s = 32.0$ mm, $P = 28.0$ kN). Contours of the maximum values (through all layers) of the effort indices were determined for these points, i.e. $R = \max_i(R_i)$, wherein $i = 1,2,3,4$ for laminates, and $i = 1,2,3,4,5,6$ for the adhesive layer. For example, Figure 8 shows a map of the maximum value of R in the composite shells, corresponding to load level L3. The contour properly reflects the 3-point bending test of a composite thin-walled box beam and shows the failure area of the top shell.

Figure 9 shows the virtual deformation of the validation segment corresponding to the crosshead displacement of $s = 200$ mm. Comparing the deformation contour with a photo from the experiment (Fig. 4), good qualitative and quantitative agreement of segment deformation can be observed.

The maximum values (through all layers) of effort indices R_1, R_2, R_3, R_4 in the composite shells (indices R_5, R_6 are not available in the applied type of shell

elements), corresponding to load levels L1, L2 and L3, are listed in Table 4. The max max values are written in bold. The max max value of the effort index for the adhesive layer, $R = \max R_i, i = 1,2,3,4,5,6$ is 0.104.

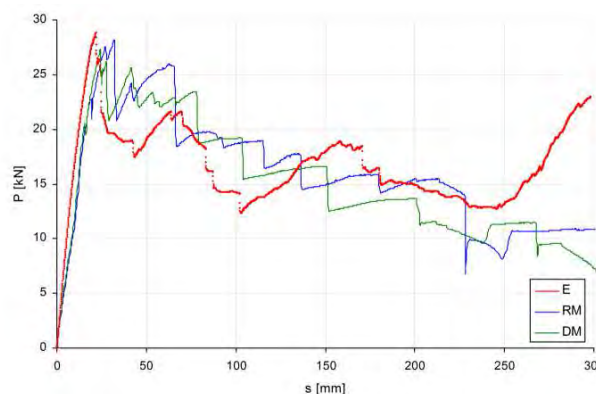


Fig. 7. $P(s)$ plots: E - experimental; RM - simulation (rare mesh); DM - simulation (dense mesh)

Rys. 7. Wykresy $P(s)$: E - eksperyment; RM - symulacja (siatka rzadka); DM - symulacja (siatka gęsta)

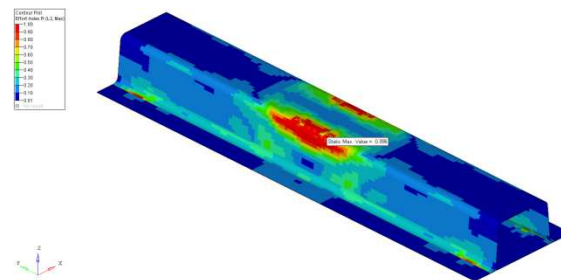


Fig. 8. Contour of maximum values of effort index R in composite shells, corresponding to load level L3

Rys. 8. Mapa maksymalnych wartości indeksu wyężenia R w powłokach kompozytowych, odpowiadająca poziomowi obciążenia L3 (skala 0÷1)



Fig. 9. Virtual deformation of validation segment, corresponding to crosshead displacement of $s = 200$ mm

Rys. 9. Wirtualna deformacja segmentu walidacyjnego, odpowiadająca przemieszczeniu trawersy $s = 200$ mm

TABLE 4. List of maximum values of effort indices R_i (maximum values are written in bold)

TABELA 4. Zestawienie maksymalnych wartości indeksów wyężenia R_i (wartości maksymalne zapisano czcionką bold)

Load level	R_1	R_2	R_3	R_4
L1	0.852	0.951	0.806	0.962
L2	0.979	0.987	0.978	0.979
L3	0.982	0.996	0.985	0.981

On the basis of conducted numerical studies, the following conclusions can be drawn:

- 1) Contours of the effort index R properly reflect the 3-point bending test of a composite box beam including the impact of the testing machine movable stamp and immovable supports.
- 2) A rigid stamp moving vertically down causes effort concentration in the central contact zone of the top shell (TS) with the stamp and in the far contact zones of the bottom shell (BS) with the lateral support plates.
- 3) Deflection of the beam segment changes contact at the support plates from the surface to the edge one. Lateral bending of the beam bottom at the supports results in quasi-point contact between the beam and the support edge.
- 4) For load level L1, the effort index of the composite segment is high and it comes to $R = 0.962$. Quasi-point concentrations of effort under the stamp (intersection of stamp transverse edges with the shell longitudinal edges), as well as close to the supports, are formed.
- 5) For load level L3, the effort index of the composite segment is very high and it comes to $R = 0.996 \approx 1$ (load capacity of segment). Quasi-linear concentrations of effort under the stamp (sections of shell longitudinal edges), as well as quasi-point concentrations of effort close to the supports, are formed. The most strenuous layers are 5 (GBX) and 6 (BAT) in the top shell (under stamp) and in the bottom shell (on support edges).
- 6) Quantitative and qualitative results allow one to interpret the L1 and L2 points on the $P(s)$ plot as points of local slight decrease in load capacity resulting from the assumed methodology of numerical modelling.
- 7) The system model for the bending test is bi-symmetric. However, the effort index contours are not perfectly bi-symmetric due to imperfections in the numerical model (an automatically generated FE mesh is not perfectly bi-symmetric).
- 8) The results in terms of $F(s)$ plots and effort indices contours positively validate the numerical modelling and simulation of the bending test of a composite beam segment.

CONCLUSIONS

Experimental and numerical studies of a composite validation box segment, consisting of two glass/vinylester shells glued together, have been conducted. Laminate shells were formed by means of infusion technology and glued one to another. The laminate components, glue (adhesive layer) and manufacturing

technology of the beam segment are similar to those for the technical object, i.e. the glued composite box foot-bridge.

A three-point bending test of the validation segment was conducted. The experimental stand was designed and built in a SATEC-1200 universal testing machine. The test was carried out to partial destruction of the segment, applying kinematic excitation with a cross-head speed of 1 mm/s and maximum vertical distance of 300 mm. The measurements included the following quantities: stamp force (P), vertical displacement of the crosshead (s), vertical displacement of the right support (to control support susceptibility), deformation of the beam segment during the test (photo documentation).

Numerical modelling and simulation of a bending test of the validation segment was conducted using FE code MSC.Marc 2010. The laminates were simulated using thick-shell elements with the orthotropic linear elastic-brittle material model for the vinylester lamina, corresponding to a single layer of orthogonal quasi-balanced stitched fabric. Numerical modelling and simulation of the static processes in the laminate shells including failure has been developed in comparison with the authors' previous works (a new type of composite material, infusion technology, composite shells glued one to another).

Acknowledgements

The study has been supported by the National Centre for Research and Development, Poland, as a part of a research project No. PBS1/B2/6/2013, realized in the period 2013–2015. This support is gratefully acknowledged.

REFERENCES

- [1] Klasztorny M., Chroscielewski J., Szurgott P., Romanowski R., Design and numerical testing of 5-box GFRP shell foot-bridge, 5th Int. Conf. on Footbridges: Past, Present & Future, London, England, 16-18 July 2014, CD Proceed., Paper #1094, 1-8.
- [2] Jones R.M., Mechanics of composite materials, Taylor & Francis, London 1999.
- [3] Tsai S.W., Composites design, 4th Edn., Think Composites, Dayton 1987.
- [4] MSC.Marc r1, Vol. A, Theory and User Information, MSC.Software Co., Santa Ana, CA, USA, 2008.
- [5] Klasztorny M., Bondyra A., Szurgott P., Nycz D., Numerical modelling of GFRP laminates with MSC.Marc system and experimental validation, Computational Material Science 2012, 64, 151-156.
- [6] Nycz D., Bondyra A., Klasztorny M., Gotowicki P., Numerical modelling and simulation of the composite segment bending test and experimental validation, Composites Theory and Practice 2012, 2(12) 126-131.